Employing refractive beam shaping in a Lloyd's interference lithography system for uniform periodic nanostructure formation

Yung-Jr Hung, Han-Jung Chang, Ping-Chien Chang, Jia-Jin Lin, and Tzu-Chieh Kao

Citation: Journal of Vacuum Science & Technology B, Nanotechnology and Microelectronics: Materials, Processing, Measurement, and Phenomena **35**, 030601 (2017); doi: 10.1116/1.4980134

View online: http://dx.doi.org/10.1116/1.4980134

View Table of Contents: http://avs.scitation.org/toc/jvb/35/3

Published by the American Vacuum Society

Employing refractive beam shaping in a Lloyd's interference lithography system for uniform periodic nanostructure formation

Yung-Jr Hung,[a] Han-Jung Chang, Ping-Chien Chang, Jia-Jin Lin, and Tzu-Chieh Kao
Department of Photonics, National Sun Yat-sen University, No. 70, Lienhai Rd., Kaohsiung 804, Taiwan

(Received 10 March 2017; accepted 3 April 2017; published 11 April 2017)

Uniform periodic structure formation over a large sample area has been challenging in laser interference lithography (LIL) mainly due to the Gaussian intensity distribution inherent to a laser beam. In this work, refractive beam shaping devices are applied in a Lloyd's interferometer to create a flat-top light field (2.8% intensity variation over an area of $20 \times 20\,cm^2$) for wafer-scale nanopatterning. Around 10^{-2} variation in fill factors are obtained for all the reported one dimensional and two dimensional periodic structures across a 2-in. wafer, which is 1 order of magnitude lower than the values obtained for the samples exposed to a Gaussian light field. The proposed LIL system also allows gradual light field transitions from the Gaussian, super-Gaussian, and flat-top to the inverse-Gaussian by simply adjusting the spot size of the laser incident to the beam shaper. The authors believe that the proposed LIL system can be applied for a variety of applications that benefit from the nature of periodic nanostructures. © *2017 American Vacuum Society*. [http://dx.doi.org/10.1116/1.4980134]

I. INTRODUCTION

Laser interference lithography (LIL) has been an effective technique for patterning regular arrays of fine features over a large sample area without the use of complex optical systems or photomasks. Among all the LIL systems, Lloyd's mirror interferometer, in which the mirror is placed perpendicular to the exposed surface to create a second beam, is the most common approach for generating finely detailed interference patterns of sufficient visibility.[1–3] The pitch of the interference patterns can be accurately controlled by placing the sample and the mirror on a rotating stage. The grating period is therefore determined by the wavelength of the laser, the angle of intersection between the mirror and the sample, and the stage orientation with respect to the direction of the laser beam. A Lloyd's mirror interferometer using an ultraviolet laser as the irradiation source is effective only for short-period (200–400 nm) grating formation. Even when using a 4-in. mirror, the illumination coverage of a Lloyd's mirror interferometer is still less than 1 in. while the grating periodicity is larger than 500 nm.[4] On the other hand, the illumination coverage for <250-nm grating periods is always larger than the size of the mirror. As a result, a LIL system equipped with a Lloyd's mirror has been widely used in the semiconductor laser industry for distributed feedback laser fabrication, which requires a precise and uniform grating periodicity of 202 or 240 nm on 2-in. III–V epiwafers for emitting 1310- or 1550-nm of telecom wavelengths. Other applications such as wire-grid polarizers for displays and silicon antireflective surfaces for solar harvesting also require closely packed one-dimensional (1D) or two-dimensional (2D) gratings distributed uniformly over a large area. However, the Gaussian distribution inherent to laser beams causes the exposure dose in a Lloyd's mirror interferometer to vary across the exposure area,[1,5] with the maximum exposure intensity occurring at the intersection between the mirror and the sample stage, as shown in Fig. 1(a). The dose variation can lead to variations in the fill factor of the resulting grating patterns. The parameter "fill factor" is defined as the volume fraction of the resist material remaining on the sample after development. In cases where a double exposure of the interference fringe is executed with the sample rotated by 0° and 90°, a 2D grating pattern with a square lattice of circular geometry can be produced. When the exposure energy is not uniform across the entire sample, the resulting 2D grating profiles can be distorted.

A two-beam interferometer allows the sample to be centered at the maximum intensity of the Gaussian beam profile, thereby allowing higher illumination intensity with a greater uniformity, as shown in Fig. 1(b). But the two-beam LIL system is rendered highly sensitive to vibration and fluctuations in air flow, thereby degrading the visibility of the resulting interference fringes.[4,6] In addition, the use of a two-beam interferometer only reduces the impact of a nonuniform light field on the resulting resist grating profile, but the on-wafer variation in the grating fill factor still exists. The conversion of the Gaussian intensity profile of a laser beam into a more uniform distribution seems to be the most straightforward way to solve this issue, as shown in Fig. 1(c). Recently, a beam flattening device based on a cascaded optical filter has been designed to obtain an optical transmittance with an inverse Gaussian shape versus incident angle. This beam flattening device is then utilized in a Lloyd's mirror interferometer to convert the divergent Gaussian laser beam into a more uniform intensity distribution.[7] However, about 10% variation in the fill factor of resultant gratings over a sample area of only 1.4-cm was still observed. In contrast, beam

[a]Electronic mail: yungjr@mail.nsysu.edu.tw

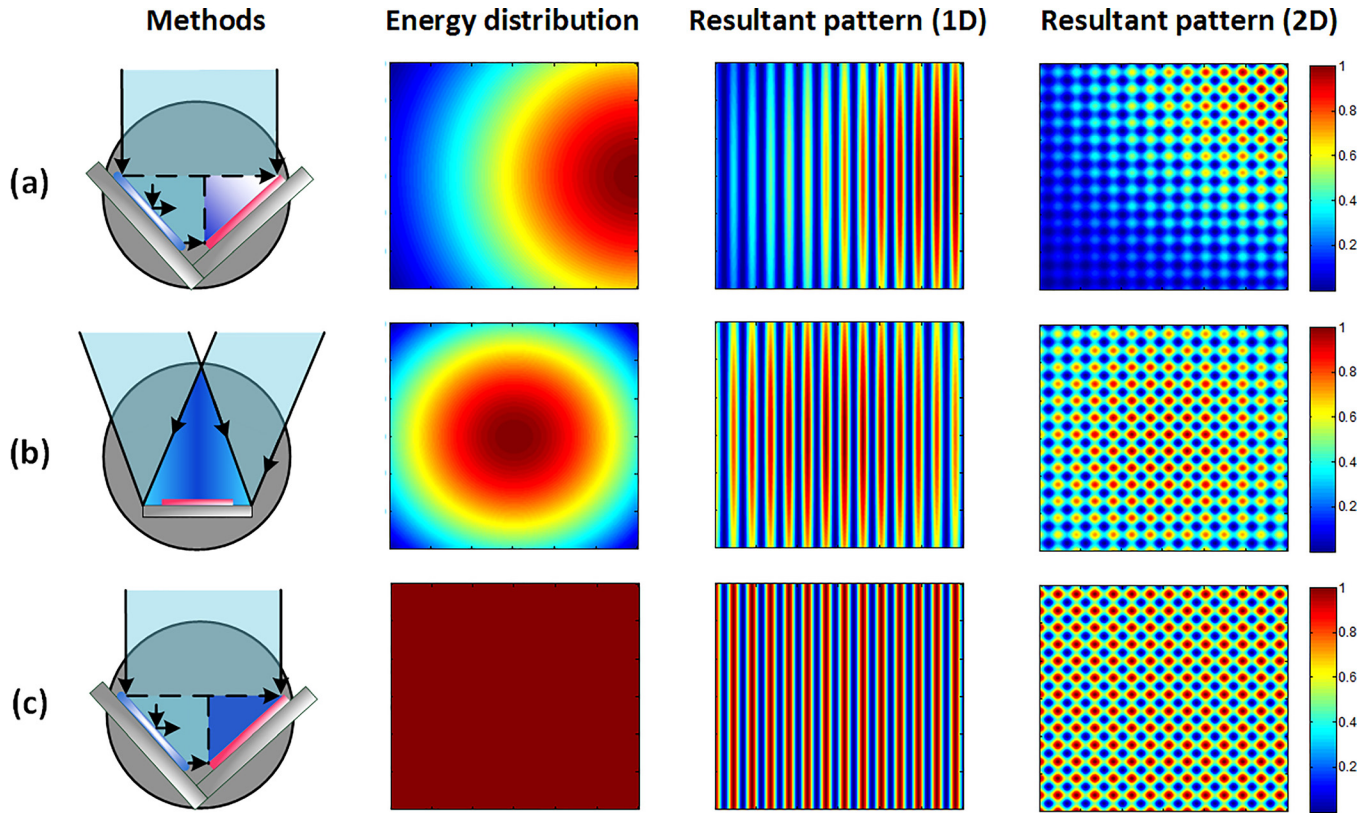

FIG. 1. (Color online) Calculated energy distribution of the laser beam on the sample and the corresponding dose modulation profiles in the formation of 1D and 2D gratings, respectively: (a) Lloyd's mirror interferometry with a Gaussian laser intensity distribution, (b) dual-beam interferometry with a Gaussian laser intensity distribution, and (c) Lloyd's mirror interferometry with a flat-top laser intensity distribution.

shaping techniques based on optical refraction have been developed for years to convert Gaussian intensity distribution into a flat-top one,[8–11] but none of them had been utilized in a LIL system to generate a flat-top laser beam for uniform nanopatterning. This paper aims to bridge this gap by utilizing a refractive beam shaper in a Lloyd's mirror interferometer to achieve an expanded and flat-top beam intensity profile for successful wafer-scale nanopatterning of 1D and 2D periodic structures with superior pattern uniformity. The variation in the fill factor of resultant 1D gratings can be as low as only 0.011 over a 2-in. sample area.

II. EXPERIMENT

Most of the He-Cd lasers widely used in interference lithography have a coherence length of only around 30 cm, which limits the useful illumination coverage to approximately 4 in. even when a larger Lloyd's mirror is employed.[4] Figure 2 presents a schematic diagram of the proposed LIL system equipped with a refractive beam shaper and a Lloyd's mirror. We adopt a 355-nm diode-pumped solid-state laser (Cobolt Zouk^{TM}) with a TEM_{00} spatial mode ($M^2 < 1.1$), an output power of 20 mW, and a coherence length exceeding 40 m (spectral linewidth <1 MHz) as the radiation source in the proposed LIL system. This laser not only has a longer coherence length than the widely used 325-nm He-Cd laser but also has a relatively compact size ($12.5 \times 7 \times 4.5$ cm). With a highly coherent laser source, the illumination coverage of a Lloyd's interferometer is therefore limited only by the size of the mirror.[4] Consequently, the variation in the fill factor of resultant resist patterns across the wafer solely depends on the intensity uniformity of the laser light field. After passing an automatic optical shutter, the laser beam then enters a volume-grating-based spatial filter to remove its aberrations, a variable optical attenuator to adjust the laser intensity, a beam shaping device to transform the Gaussian intensity profile of a laser beam into a uniform one, and a planoconcave lens to expand the light field for the following interference taking place at the Lloyd's

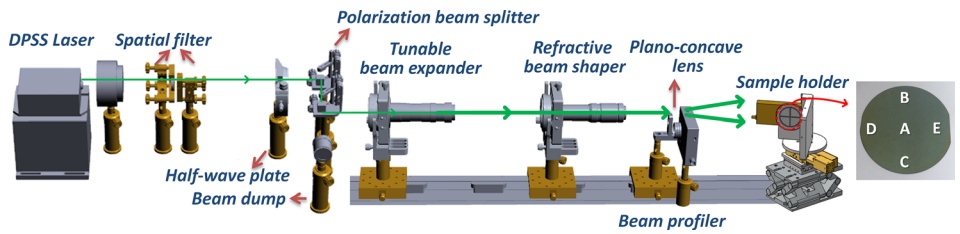

FIG. 2. (Color online) Schematic diagram of the proposed Lloyd's mirror interferometer with a flat-top laser intensity distribution.

mirror interferometer. The variable optical attenuator consists of a half-wave plate and two polarizing cube beamsplitters, while the beam shaping device is composed of a tunable beam expander and a refractive beam shaper. The refractive field-mapping beam shaper (πshaper from AdlOptica GmbH) is implemented as a Galilean telescopic system with two aspheric lenses. The transformation of the intensity profile from the Gaussian to the flat-top is realized in a controlled manner by accurately introducing wave aberration by the first lens and further its compensation by the second lens. Thus, the resulting output beam has a uniform irradiance profile, a flat wavefront, and a low divergence. In other words, the beam shaper transforms the irradiance distribution without the deterioration of the wavefront shape or increasing the beam divergence. The deviation from flatness for the output phase front is less than one tenth of the laser wavelength. However, the successful transformation of a laser irradiance distribution requires the fulfillment of a predetermined input beam size with a Gaussian-like irradiance distribution. It is also important to ensure the proper alignment of the beam shaper to avoid the lateral shift of a laser beam or angular tilt of the beam shaper, all leading to a skewed intensity profile. In this work, a tunable beam expander is utilized to enlarge the laser beam size from originally 0.7–6 mm in order to obtain a uniform irradiance profile after passing the beam shaper. A beam profiler is used to assist the alignment of the beam shaper through *in situ* measurements of the transformed irradiance profile of the laser beam. Since the saturation intensity for the beam profiler is only 2.2 μW/cm^2, it is necessary to attenuate the output power of the laser beam without changing its spot size during the alignment of the beam shaper, which describes a polarization-based variable optical attenuator. We cascade two polarizing cube beamsplitters after the half-wave plate to achieve an extinction ratio of $>$40 000 for ultraviolet light such that the laser power can be attenuated to be within the operational intensity of the beam profiler while maintaining the s-polarization of the laser beam and its spot size.

When a TEM$_{00}$ laser beam with Gaussian irradiance distribution propagates in space, its size varies due to inherent beam divergence but its irradiance distribution remains stable. However, when light beams with non-Gaussian irradiance distributions such as flat-top beams propagate in space, they simultaneously show a variation in both the size and the irradiance profile. In infinity, the profile of the laser beam becomes the well-known "Airy disk" distribution, which is the result of the Fourier-Bessel transform for a circular beam of uniform initial irradiance.[12–14] There exists, however, a certain propagation length where the uniform intensity profile is relatively stable. This length is inversely proportional to the wavelength and is in square proportional to the beam size. Coincidentally, for the interference lithography application, we also need an expanded laser beam of uniform intensity whose coverage is a lot larger than the output beam size of a refractive beam shaper. As a result, a planoconcave lens is used in the proposed LIL system for light expansion after beam shaping not only to extend the "depth of field" after the beam shaper where the resulting irradiance profile is stable but also to obtain an enlarged laser beam for wafer-scale nanopatterning. Finally, an expanded and uniform light field illuminates a Lloyd's mirror interferometer equipped with a 3-in. dielectric mirror to generate interference fringes.

For experimental demonstrations, we have produced a variety of 1D and 2D resist grating patterns over 2-in. silicon wafers. The fabrication flow is outlined as follows. A 160-nm-thick bottom antireflection coating (BARC) (Brewer Science iCON-16) layer was deposited on a cleaned silicon substrate by spin coating. After prebaking the BARC layer at 165 °C for 60 s, a 200-nm-thick positive layer of photoresist (TOK THMR-iP3600) was deposited and soft baked at 90 °C for 90 s. The sample was then transferred to the LIL system and exposed to interference fringes with a suitable dose during each exposure step. The periodicity of as-realized 1D gratings is around 240 nm. The exposure energy for 1D gratings is about 28 mJ/cm^2. Employing multiexposures of interference fringes with the sampled rotated by (0°, 90°), (0°, 60°, −60°), (0°, 45°, 90°, 135°), (0°, 36°, 72°, 108°, 144°), and (0°, 30°, 60°, 90°, 120°, 150°) would form 2D gratings with an orientation of square, hexagonal, and higher rotational symmetries (eightfold, tenfold, and 12-fold), respectively. The energy for each exposure step from square and hexagonal 2D gratings is about 22 mJ/cm^2. For gratings with higher rotational symmetries (eightfold, tenfold, and 12-fold), the energy is reduced to only 4–6 mJ/cm^2 for each exposure. For comparison, all the 2D gratings are generated with the same interference angle of 30°. Postexposure baking was performed at 110 °C for 120 s to reduce the standing-wave effect. Finally, the sample was immersed in a standard 2.38% tetramethylammonium hydroxide photoresist developer for 10 s to produce the grating structures. Although the interference fringe has a sinusoidal intensity profile, we can still produce resist gratings with a squarelike profile by operating the photoresist in strong nonlinear conditions.[3,15–17] This trick works for not only 1D gratings but also 2D gratings with a square or hexagonal lattice. The formation of 2D resist gratings with a rotational symmetry of eightfold or higher requires at least four exposures to interference fringes. This leads to at least four different levels of exposure doses in the resultant photoresist patterns. Therefore, such a complex grating structure can only be formed by operating the photoresist in linear conditions.

III. RESULTS AND DISCUSSION

The operation principle of a refractive beam shaper used in the proposed LIL system presumes that a perfect Gaussian beam with a 1/e^2 diameter of 6 mm is converted to a beam with uniform intensity. Figure 3(a) shows the measured beam intensity profiles of the original laser beam and the laser beams after shaping. When the input beam size is exactly 6 mm, the output laser beam has a flat-top intensity profile after passing the refractive beam shaper. The increase in the input beam size to 7.1 mm leads to a reduced intensity in the center of the output laser beam, thus generating a laser beam with the so-called inverse-Gaussian intensity profile. In contrast, the size reduction of the input laser beam to 4.9 mm enables a convex intensity profile in the output laser beam that can be approximately described by super-Gaussian

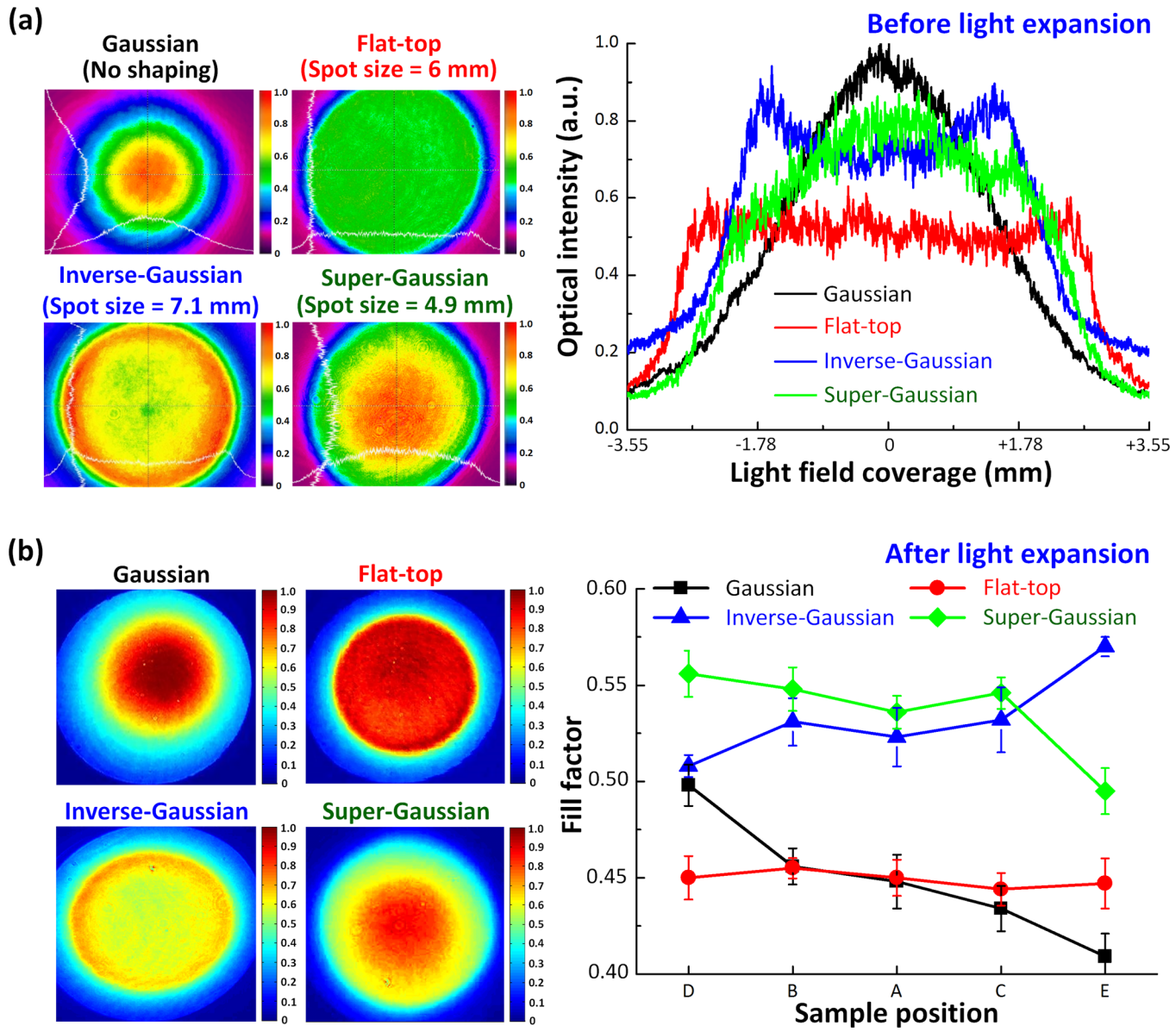

FIG. 3. (Color online) (a) Measured beam intensity profiles before light expansion under different spot sizes of the input laser beams. (b) Measured beam intensity profiles after light expansion and the corresponding fill factors of the resultant grating profiles.

functions. Evidently, a simple variation in the laser beam size by using a zoom beam expander allows us to steadily vary the resulting beam profile and choose an optimum one for specific applications. For example, large-area formation of uniform grating structures by using a Lloyd's interferometer requires a flat-top intensity profile of the laser beam. But the formation of gradient-period grating structures may need an inverse-Gaussian intensity profile due to the difference in exposure energy required for short- and long-period gratings.[18,19] After light expansion by a plano-concave lens, the light field covers an area of $20 \times 20\,\mathrm{cm}^2$ sufficient to illuminate the entire sample holder while maintaining its intensity profile, as shown in Fig. 3(b). We clearly observe that after light expansion, a flat-top laser beam can provide a uniform light field area ($L = 12.5$ cm) that is two times larger than that provided by a Gaussian laser beam ($L = 5.5$ cm). The optical power variation from the center to the edge of an expanded Gaussian laser beam can be as high as 34.5%. When this nonuniform light field is utilized in a LIL system, the sample holder is usually positioned far away from the planoconcave lens so that only the central maximum of the light field exposes to the sample area. The approximately parabolic shape near the maximum dictates that an increase in the width by a factor of two results in an improvement in uniformity by approximately a factor of four. But this also leads to a reduced intensity by a factor of four—the tradeoff in a conventional LIL system. In contrast, the optical power variation from the center to the edge of an expanded flat-top laser beam after refractive beam shaping is reduced to only 2.8%, making this light field highly desirable for LIL applications.

All light fields (named Gaussian, flat-top, inverse-Gaussian, and super-Gaussian) generated by the refractive beam shaper are applied in a Lloyd's mirror interferometer

with their beam centers aligned to the intersection between the mirror and the sample stage. Figure 3(b) reveals the variation in the fill factor of as-recorded resist gratings across the 2-in. wafer in which the sample positions A, B, C, D, and E correspond to the center, top, bottom, left, and right (major cut) of the wafer, respectively, and the major cut edge is positioned close to the intersection of the sample stage. When a Gaussian light field is used to generate interference fringes, sample position E receives the highest exposure dose while sample position D has the least. This leads to a gradually changed fill factor of resultant gratings across the wafer from 0.5 at position E to 0.41 at position D, corresponding to a variation of 0.09 in the fill factor. The use of a super-Gaussian light field still leads to a nonuniform grating pattern but with a reduced variation of 0.06 in the fill factor (from 0.55 at position E to 0.49 at position D). As the interference fringes come from the light field with an inverse-Gaussian intensity distribution, sample position E then receives the least exposure dose among all the positions. This otherwise leads to the highest fill factor of 0.57 at sample position E and the lowest fill factor of 0.5 at sample position D, corresponding to a 0.07 fill factor variation across the 2-in. wafer. Uniform gratings with an almost constant fill factor of 0.45 (about 0.011 variation in the fill factor across the 2-in. wafer) can be finally achieved by employing a flat-top light field.

To further validate the advantages of a flat-top beam profile in a Lloyd's mirror interferometer, 2D grating structures with a hexagonal lattice are realized by triple exposures to the interference fringes and the rotation of the sample by 60° and −60°, respectively, before the second and third exposure, as illustrated in Fig. 4(a). Prior to grating fabrication, a simulation model is built to calculate the profiles of holographically recorded patterns to initially understand the effects of each process parameter.[3] Typically, the profile of recorded structures in the photoresist depends on the interference pattern and photoresist sensitization and development.[3] Figures 4(b)–4(e) show the calculated light intensity

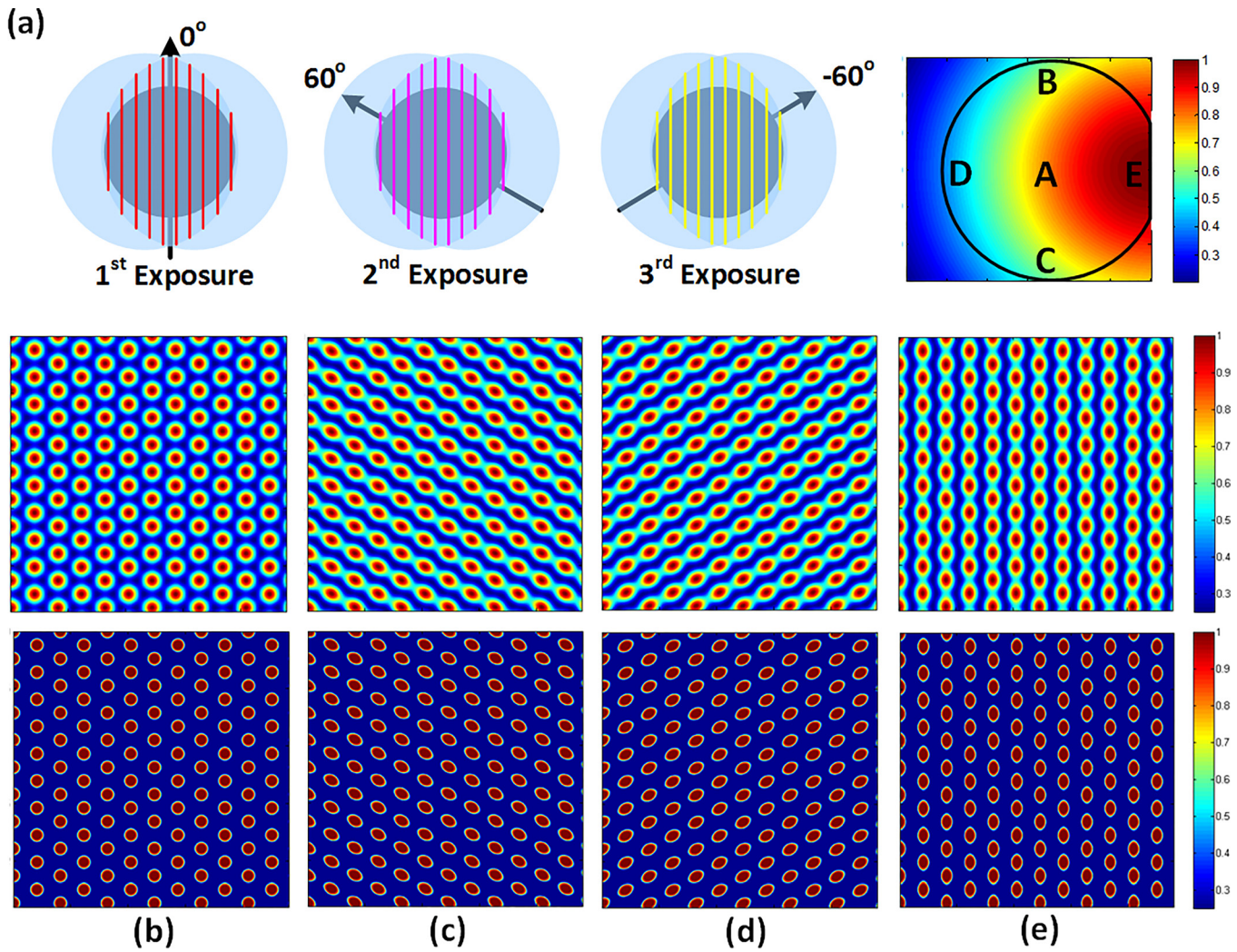

FIG. 4. (Color online) (a) LIL process procedures for forming hexagonal 2D grating structures by triple exposures to 1D interference fringes generated by a Lloyd's mirror interferometer and the sample rotated by 60° and −60°, respectively, before the second and third exposure. Assuming a Gaussian intensity distribution for the incident light field, the exposure energy received at respective wafer positions (A, B, C, D, and E) varies during the triple-exposure step. (b)–(e) Calculated light intensity distributions under triple-exposure of two-beam interference (upper figures) and their resultant resist patterns after development (lower figures) at respective wafer positions (A, B, C, and E).

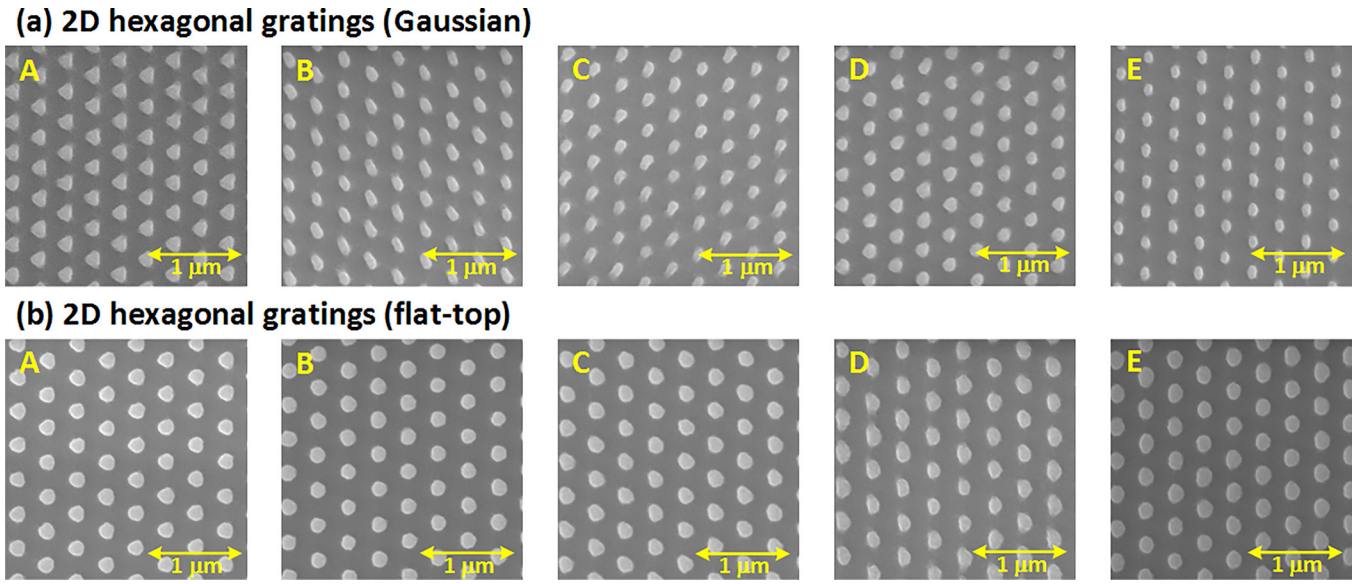

FIG. 5. (Color online) Top SEM views of as-realized 2D hexagonal gratings realized by employing (a) a Gaussian light field or (b) a flat-top light field.

distributions under triple-exposure of two-beam interference and their resultant resist patterns after development at respective wafer positions (A, B, C, and E). Hexagonal 2D gratings with a circular geometry are realized at position A [Fig. 4(a)] since the exposure energy remains almost the same during the triple-exposure LIL process. In contrast, Gaussian intensity distribution combined with the sample rotation leads to the variation in exposure energy at other wafer positions and thus distorts the resultant grating profile. Elliptical 2D gratings with their major-axis along the vertical direction shown in Fig. 4(e) can be found at sample position E. Such a distorted profile is attributed to a higher exposure energy at the first exposure step than that of the second and third exposures. Similarly, elliptical 2D gratings with a tilted major-axis direction are found at sample positions B and C, as shown in Figs. 4(c) and 4(d). The resultant resist pattern profile at sample position D is similar to that at sample position E but the exposure energy difference among three exposure steps at position D is not as large as that at position E. So, the profile distortion of the resist patterns at position D is not obvious. For experimental demonstration, a BARC layer is used to avoid the interface reflection of incident UV light between the substrate and the photoresist and thus eliminates the standing wave effect that may distort the resist profile. As a result, the profile of resulting 2D gratings would loyally reflect the spatial intensity variation of the incident light field. Figure 5(a) shows the top SEM views of as-realized hexagonal 2D gratings over a 2-in. wafer generated by a Gaussian light field. The impacts of Gaussian intensity distribution on the resultant resist profiles are verified experimentally, and the results agree well with the theoretical predictions shown in Fig. 4. The pattern distortion on square 2D gratings produced by the double-exposure of two-beam interference with a sample rotation of 90° before the second exposure is also observed.[20] If a uniform light field is used for the triple-exposure LIL process, 2D hexagonal gratings with a circular geometry can be realized throughout the entire sample area, as verified experimentally in Fig. 5(b). We therefore characterize the fill factor and ellipticity (e) of the 2D hexagonal gratings to quantify its wafer-scale uniformity. The results on square and hexagonal 2D gratings are revealed in Fig. 6. With a Gaussian light field, the variations in the fill factor and ellipticity are as high as 0.093 (0.105) and 0.57 (0.59) for resultant hexagonal (square) 2D gratings,

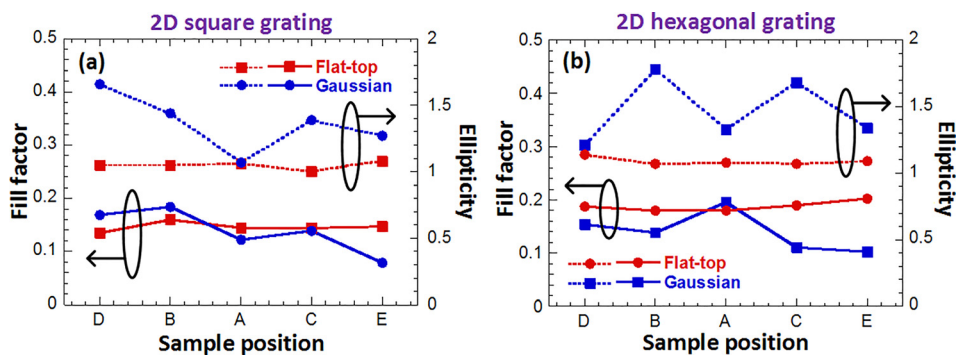

FIG. 6. (Color online) Fill factor and ellipticity of as-realized (a) 2D square-oriented gratings and (b) 2D hexagonal-oriented gratings at different sample positions across a 2-in. wafer.

respectively, across a 2-in. wafer area. However, when a flat-top light field is employed, the fill factor and ellipticity variation can be reduced to 0.023(0.025) and 0.07(0.08) for hexagonal (square) 2D gratings, respectively, showing its great promise for wafer-scale nanopatterning applications.

Photonic quasicrystals are promising nanostructures due to their superior photonic bandgap properties stemming from their higher rotational symmetries. The formation of 2D quasicrystals with a rotational symmetry of eightfold or higher can be achieved by the multiple-exposure LIL process, but this process is very sensitive to the exposure dose variation.[21] The as-realized 2D quasicrystals can further serve as a phase mask to realize 3D quasicrystals.[22] With a light field having a flat-top intensity distribution, the proposed Lloyd's LIL system is suitable to pattern 2D quasicrystal structures uniformly over a large area. Figure 7 shows the calculated light intensity distributions, resultant resist patterns after development, and the SEM views of the as-realized 2D quasicrystals with an orientation of square (fourfold), hexagonal (sixfold), and higher rotational symmetries (eightfold, tenfold, and 12-fold). Leveraging from the nonlinear photoresist response, isolated pillar arrays with a square or hexagonal orientation can be achieved even though three different intensity levels (nonexposed region, single-exposed region, and double-exposed region) are distributed during the multiexposure LIL process.[3] In this case, the energy of each exposure exceeds the energy threshold of the photoresist such that the dissolution rate of the photoresist in a developer is high in both single- and double-exposed regions. Therefore, exposure to a nonuniform Gaussian light field would mainly lead to the shape distortion in resultant patterns, thus causing a variation in the fill factor. Alternatively, since more than four exposure steps are required to form 2D quasicrystals with a rotational symmetry of eightfold and higher, the energy of each exposure step is not high enough to activate the dissolution process of the photoresist in a developer. Instead, the superposition of interference fringes for forming high-symmetry 2D quasicrystals would add up the exposure energy to reach the threshold of the photoresist to be able to dissolve in a developer.

Figure 8 shows the fill factor variation of as-realized high-symmetry 2D quasicrystals (eightfold, tenfold, and 12-fold) across a 2-in. wafer. The impact of the nonuniform Gaussian light field in the resultant high-symmetry 2D quasicrystals is not on their shape distortion but mainly on their aspect ratio variation (the difference in the resist thickness). So, we observe the variation not only in the fill factor of resultant patterns but also in the image contrast during SEM characterization across the entire wafer. With a Gaussian light field, generally the sample positions A and C will receive the highest exposure energy while sample position B will receive the least exposure energy. The exposure energy at positions D and E is similar and is slightly higher than the energy at position B. After the multiexposure LIL process, the resultant 2D quasicrystal patterns (eightfold, tenfold, and 12-fold) are characterized to have the lowest fill factor at

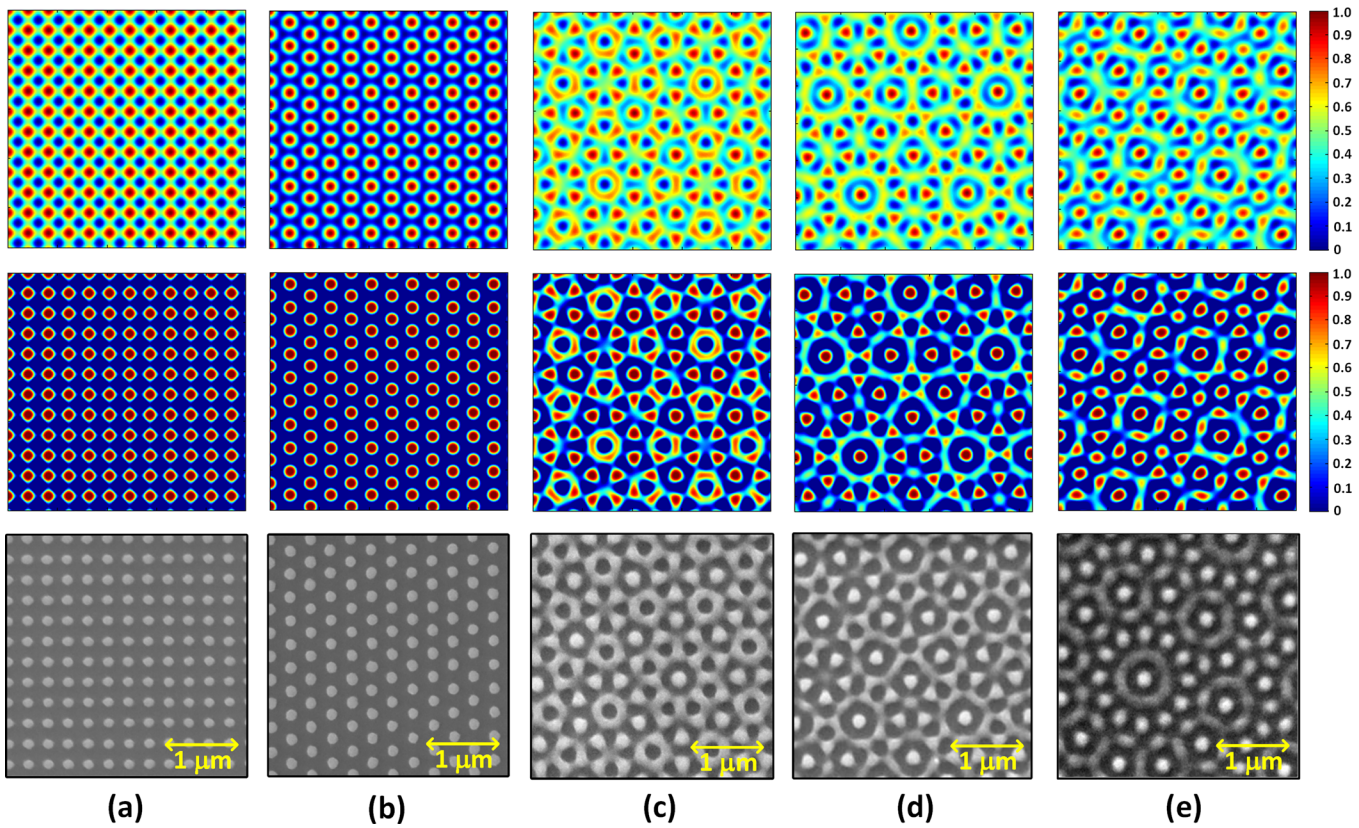

FIG. 7. (Color online) Calculated light intensity distributions (top), resultant resist patterns after development (middle), and SEM views of as-realized resist patterns (bottom): (a) fourfold (square-oriented), (b) sixfold (hexagonal-oriented), (c) eightfold, (d) tenfold, and (e) 12-fold quasiperiodic nanostructures.

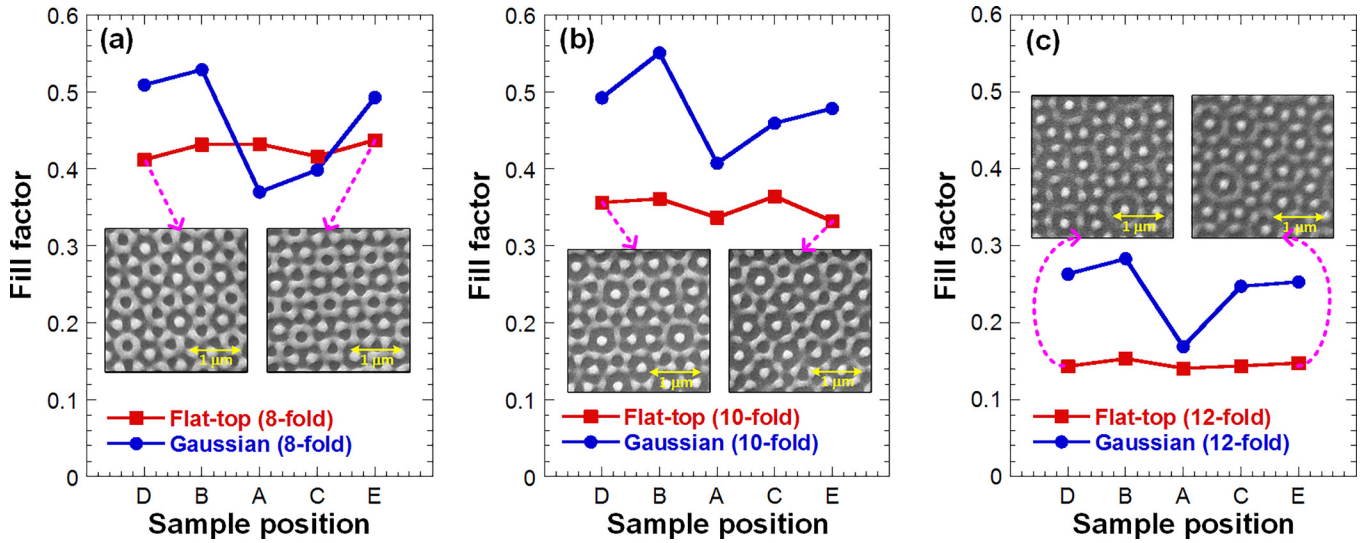

FIG. 8. (Color online) Fill factor of as-realized 2D quasicrystals with a rotational symmetry of (a) eightfold, (b) tenfold, and (c) 12-fold at different sample positions across a 2-in. wafer. (The red line with filled square symbols represents a flat-top light field while the blue line with filled circular symbols represents a Gaussian light field.)

position A and the highest fill factor at position B. Therefore, the variation in the fill factor is as high as 0.1588, 0.1433, and 0.1141 for eightfold, tenfold, and 12-fold quasicrystals, respectively, across a 2-in. wafer. When a flat-top light field is utilized in the multiexposure LIL process, the fill factor variation is then reduced to 0.0158, 0.0322, and 0.013 for eightfold, tenfold, and 12-fold quasicrystals, respectively, across a 2-in. wafer.

IV. CONCLUSIONS

In this work, we have proposed and demonstrated a laser interference lithography system capable of providing a flat-top beam intensity profile for wafer-scale nanopatterning. This LIL system is based on simple Lloyd's mirror configuration but equipped with additional refractive beam shaping devices to transform the Gaussian intensity profile of a laser beam into a uniform one. After light expansion, the light field covers an area of $20 \times 20\,\mathrm{cm}^2$ with an intensity variation of only 2.8%, which is 1 order of magnitude lower than the intensity variation from a Gaussian light field. Uniform 1D gratings with an almost constant fill factor (0.45 ± 0.011) and periodicity (240 ± 0.37 nm) are realized across a 2-in. wafer, which are ready for distributed feedback semiconductor laser fabrication for telecommunication applications. By conducting a multiple-exposure LIL process on a flat-top light field, uniform 2D gratings with a hexagonal lattice are achieved with their variations in the fill factor and ellipticity of only 0.023 and 0.025 across a 2-in. wafer, which is 1 order of magnitude lower than the values obtained from the samples exposed to a Gaussian light field. Such 2D gratings can be applied to fabricate patterned sapphire substrates for light-emitting diode applications. We also obtain 10^{-2} fill factor variations from photonic quasicrystals having a rotational symmetry of eightfold and higher. The exposure area of the current LIL system in this demonstration is limited by the size of Lloyd's mirror and can be upgraded to cover an even larger sample area (4-in. or larger) without compromise.[4] Finally, the proposed LIL system allows gradual light field transitions from the Gaussian, super-Gaussian, and flat-top to the inverse-Gaussian, by simply controlling the spot size of the laser incident on the beam shaper, making this system more flexible for various applications.

ACKNOWLEDGMENTS

The authors would like to acknowledge Alexander Laskin of AdlOptica GmbH for his helpful discussions. This work was supported in part by the Ministry of Science and Technology, Taiwan, under Grant Nos. MOST102-2218-E-110-010, MOST103-2221-E-110-038, MOST104-2221-E-110-061, and MOST105-2221-E-110-075.

[1]E. Ertorer, F. Vasefi, J. Keshwah, M. Najiminaini, C. Halfpap, U. Langbein, J. J. L. Carson, D. W. Hamilton, and S. Mittler, J. Biomed. Opt. **18**, 035002 (2013).
[2]I. Wathuthanthri, W. Mao, and C.-H. Choi, Opt. Lett. **36**, 1593 (2011).
[3]Y.-J. Hung, S.-L. Lee, Y.-T. Pan, B. J. Thibeault, and L. A. Coldren, J. Vac. Sci. Technol., B **28**, 1030 (2010).
[4]Y.-J. Hung, P.-C. Chang, Y.-N. Lin, and J.-J. Lin, J. Vac. Sci. Technol., B **34**, 040609 (2016).
[5]T. B. O'Reilly and H. I. Smith, J. Vac. Sci. Technol., B **26**, 2131 (2008).
[6]W. Mao, I. Wathuthanthri, and C.-H. Choi, Opt. Lett. **36**, 3176 (2011).
[7]Y.-K. Yang, Y.-X. Wu, T.-H. Lin, C.-W. Yu, and C.-C. Fu, Proc. SPIE **9736**, 97360Y (2016).
[8]F. Duerr and H. Thienpont, Opt. Express **22**, 8001 (2014).
[9]B. R. Frieden, Appl. Opt. **4**, 1400 (1965).
[10]J. A. Hoffnagle and C. M. Jefferson, Appl. Opt. **39**, 5488 (2000).
[11]A. Laskin, V. Laskin, and A. Ostrun, Proc. SPIE **9200**, 92000E (2014).
[12]J. W. Goodman, *Introduction to Fourier Optics* (McGraw-Hill, New York, 1996).
[13]M. Born and E. Wolf, *Principles of Optics* (Cambridge University, Cambridge, 1999).
[14]W. J. Smith, *Modern Optical Engineering* (McGraw-Hill, New York, 2000).
[15]D. J. Kim, W. G. Oldham, and A. R. Neureuther, IEEE Trans. Electron Devices **31**, 1730 (1984).

[16]B. de, A. Mello, I. F. da Costa, C. R. A. Lima, and L. Cescato, Appl. Opt. **34**, 597 (1995).
[17]A. S. Kewitsch and A. Yariv, Appl. Phys. Lett. **68**, 455 (1996).
[18]H. Kim, H. Jung, D.-H. Lee, K. B. Lee, and H. Jeon, Appl. Opt. **55**, 354 (2016).
[19]K. Liu, H. Xu, H. Hu, Q. Gan, and A. N. Cartwright, Adv. Mater. **24**, 1604 (2012).
[20]H.-J. Chang, P.-C. Chang, and Y.-J. Hung, *Proceedings of the Conference on Lasers and Electro-Optics (CLEO)*, San Jose, CA (2016), Paper No. SM2R.7.
[21]N. D. Lai, J. H. Lin, Y. Y. Huang, and C. C. Hsu, Opt. Express **14**, 10746 (2006).
[22]I. Bita, T. Choi, M. E. Walsh, H. I. Smith, and E. L. Thomas, Adv. Mater. **19**, 1403 (2007).